

GRB 081007 AND GRB 090424: THE SURROUNDING MEDIUM, OUTFLOWS AND SUPERNOVAE

ZHI-PING JIN^{1,2}, STEFANO COVINO¹, MASSIMO DELLA VALLE^{3,4}, PATRIZIA FERRERO^{5,6}, DINO FUGAZZA¹, DANIELE MALESANI⁷, ANDREA MELANDRI¹, ELENA PIAN^{8,9}, RUBEN SALVATERRA¹⁰, DAVID BERSIER¹¹, SERGIO CAMPANA¹, ZACH CANO¹², ALBERTO J. CASTRO-TIRADO¹³, PAOLO D'AVANZO¹, JOHAN P. U. FYNBO⁷, ANDREJA GOMBOC¹⁴, JAVIER GOROSABEL^{13,15,16}, CRISTIANO GUIDORZI¹⁷, JOSHUA B. HAISLIP¹⁸, JENS HJORTH⁷, SHIHO KOBAYASHI¹¹, AARON P. LACLUYZE¹⁸, GIANNI MARCONI¹⁹, PAOLO A. MAZZALI^{11,20,21}, CAROLE G. MUNDELL¹¹, SILVIA PIRANOMONTE²², DANIEL E. REICHART¹⁸, RUBÉN SÁNCHEZ-RAMÍREZ¹³, ROBERT J. SMITH¹¹, IAIN A. STEELE¹¹, GIANPIERO TAGLIAFERRI¹, NIAL R. TANVIR²³, STEFANO VALENTI²¹, SUSANNA D. VERGANI¹, THOMAS VESTRAND²⁴, EMMA S. WALKER^{8,25} AND PRZEMEK WOŹNIAK²⁴

Draft version August 27, 2024

ABSTRACT

We discuss the results of the analysis of multi-wavelength data for the afterglows of GRB 081007 and GRB 090424, two bursts detected by *Swift*. One of them, GRB 081007, also shows a spectroscopically confirmed supernova, SN 2008hw, which resembles SN 1998bw in its absorption features, while the maximum magnitude may be fainter, up to 0.7 mag, than observed in SN 1998bw. Bright optical flashes have been detected in both events, which allows us to derive solid constraints on the circumburst-matter density profile. This is particularly interesting in the case of GRB 081007, whose afterglow is found to be propagating into a constant-density medium, yielding yet another example of a gamma-ray burst (GRB) clearly associated with a massive star progenitor which did not sculpt the surroundings with its stellar wind. There is no supernova component detected in the afterglow of GRB 090424, likely because of the brightness of the host galaxy, comparable to the Milky Way. We show that the afterglow data are consistent with the presence of both forward- and reverse-shock emission powered by relativistic outflows expanding into the interstellar medium. The absence of optical peaks due to the forward shock strongly suggests that the reverse-shock regions should be mildly magnetized. The initial Lorentz factor of outflow of GRB 081007 is estimated to be $\Gamma \sim 200$, while for GRB 090424 a lower limit of $\Gamma > 170$ is derived. We also discuss the prompt emission of GRB 081007, which consists of just a single pulse. We argue that neither the external forward-shock model nor the shock-breakout model can account for the prompt emission data and suggest that the single-pulse-like prompt emission may be due to magnetic energy dissipation of a Poynting-flux-dominated outflow or to a dissipative photosphere.

Subject headings: gamma-ray burst: individual (GRB 081007, GRB 090424) - supernovae: individual (SN 2008hw) - ISM: jets and outflows

¹ INAF-Osservatorio Astronomico di Brera, via Emilio Bianchi 46, I-23807 Merate (LC), Italy

² Key Laboratory of Dark Matter and Space Astronomy, Purple Mountain Observatory, Chinese Academy of Sciences, Nanjing 210008, China jin@pmo.ac.cn

³ INAF-Osservatorio Astronomico di Capodimonte, Salita Moiariello 16, I-80131 Napoli, Italy

⁴ International Center for Relativistic Astrophysics Network, Piazza della Repubblica 10, I-65122 Pescara, Italy

⁵ Instituto de Astrofísica de Canarias (IAC), E-38200 La Laguna, Tenerife, Spain

⁶ Departamento de Astrofísica, Universidad de La Laguna (ULL), E-38205 La Laguna, Tenerife, Spain

⁷ Dark Cosmology Centre, Niels Bohr Institute, University of Copenhagen, Juliane Maries Vej 30, DK-2100 Copenhagen Ø, Denmark

⁸ Scuola Normale Superiore di Pisa, Piazza dei Cavalieri 7, I-56126 Pisa, Italy

⁹ INAF-Istituto di Astrofisica Spaziale e Fisica Cosmica, via P. Gobetti 101, I-40129 Bologna, Italy

¹⁰ INAF-IASF Milano, via E. Bassini 15, I-20133 Milano, Italy

¹¹ Astrophysics Research Institute, Liverpool John Moores University, Liverpool Science Park, 146 Brownlow Hill, Liverpool L3 5RF, UK

¹² Centre for Astrophysics and Cosmology, Science Institute, University of Iceland, Reykjavik, Iceland

¹³ Instituto de Astrofísica de Andalucía (IAA-CSIC), Glorieta de la Astronomía s/n, E-18008, Granada, Spain

¹⁴ Mathematics & Physics, University of Ljubljana, Jadranska ulica 19, 1000 Ljubljana, Slovenia

¹⁵ Unidad Asociada Grupo Ciencia Planetarias UPV/EHU-IAA/CSIC, Departamento de Física Aplicada I, E.T.S. Ingeniería, Universidad del País Vasco UPV/EHU, Alameda de Urquijo s/n, E-48013 Bilbao, Spain

¹⁶ Ikerbasque, Basque Foundation for Science, Alameda de Urquijo 36-5, E-48008 Bilbao, Spain

¹⁷ Department of Physics, University of Ferrara, via Saragat 1, I-44122 Ferrara, Italy

¹⁸ Department of Physics and Astronomy, University of North Carolina, Chapel Hill NC 27599, USA

¹⁹ European Southern Observatory, Casilla 19001, Santiago, Chile

²⁰ Max-Planck-Institut für Astrophysik, Karl-Schwarzschildstr. 1, D-85748 Garching, Germany

²¹ INAF-Osservatorio Astronomico di Padova, Vicolo dell'Osservatorio 5, I-35122 Padova, Italy

²² INAF-Osservatorio Astronomico di Roma, via Frascati 33, I-00040 Monte Porzio Catone, Roma, Italy

²³ Department of Physics and Astronomy, University of Leicester, Leicester LE1 7RH, UK

²⁴ Space and Remote Sensing, Los Alamos National Laboratory, MS-B244, Los Alamos, NM 87545, USA

²⁵ Yale University, Department of Physics, 217 Prospect Street, New Haven, CT 06511, USA

1. INTRODUCTION

Thanks to the rapid localization of gamma-ray bursts (GRBs) by the *Swift* satellite (Gehrels et al. 2004), the response of ground-based observations of GRB afterglows has been greatly enhanced and observations of GRB afterglows have become routinely possible within minutes after the explosion. Very early afterglow data are required to estimate the initial bulk Lorentz factor of the ejecta (Molinari et al. 2007), probe the physical composition of the outflow (Fan et al. 2002; Zhang et al. 2003), and constrain the density profile of the medium surrounding the progenitor (Jin & Fan 2007; Schulze et al. 2011). Late afterglow observations provide us with clues on the medium density profile, which, in turn, may provide hints on the nature of the progenitor star.

The idea that supernova (SN) explosions may also produce energetic gamma-ray emission by some mechanism goes back to Colgate (1968), but the first piece of evidence supporting such a connection was not found until 1998 (Galama et al. 1998). The connection was finally established in 2003 when SN 2003dh and SN 2003lw were unambiguously detected spectroscopically following the nearby GRB 030329 and GRB 031203, respectively (Hjorth et al. 2003; Stanek et al. 2003; Malesani et al. 2004). So far, spectral SN features have been found for only about a dozen GRBs (for recent reviews see Hjorth et al. 2012; Della Valle 2011). Current data suggest that less than 3% of Type Ib/c SNe are able to produce GRBs following the core collapse of their progenitor star (Guetta & Della Valle 2007; Soderberg et al. 2010; Ghirlanda et al. 2013).

In this work we present and discuss data of GRB 081007 and GRB 090424. Because of their occurrence at relatively low redshifts, 0.53 and 0.54, respectively, their follow-up in the optical and near-infrared (NIR) bands was particularly effective (see cases of GRBs at similar redshifts reported by Della Valle et al. 2006; Cano et al. 2011; Berger et al. 2011; Filgas et al. 2011; Troja et al. 2012; Sparre et al. 2011). We were able to detect a SN component in the late afterglow of GRB 081007.

GRB 081007 triggered the Burst Alert Telescope (BAT) onboard *Swift* on 2008 October 7 at 05:23:52 UT. It was a long GRB with a peak ~ 9 s duration in the 15-350 keV gamma-ray band (Markwardt et al. 2008). This burst also triggered the Gamma-ray Burst Monitor, onboard *Fermi*, in the 25-900 keV gamma-ray band. The prompt emission consisted of a single pulse with an estimated duration T_{90} of about 12 s (Bissaldi et al. 2008). The *Swift* satellite immediately slewed to the field and the X-Ray Telescope (XRT) and the Ultraviolet/Optical Telescope (UVOT) started observations at 99 and 108 s after the trigger, leading to a detection of the X-ray and optical afterglows (Baumgartner et al. 2008). Gemini-South took two 900 s spectra, starting 73 minutes after the burst. Two absorption lines at 6016.7 and 6070.3 Å and an emission line at 5700.9 Å were identified as Ca II H, K and [O II] 3727 Å lines respectively at $z = 0.5295 \pm 0.0001$ (Berger et al. 2008, see also figure 1).

GRB 090424 triggered BAT on 2009 April 24 at 14:12:09 UT. It was a multi-pulse long GRB with total duration of about 60 s in the 15-350 keV gamma-ray band

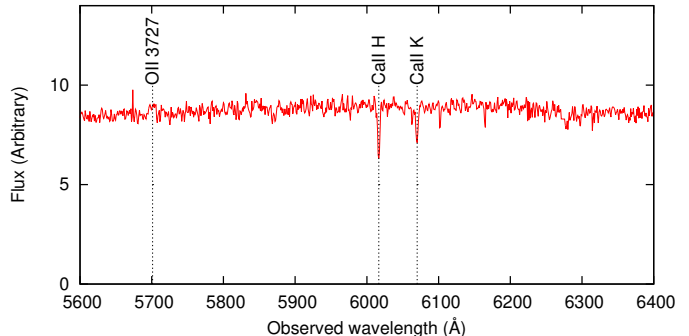


FIG. 1.— Gemini-South GMOS spectrum of GRB 081007 afterglow.

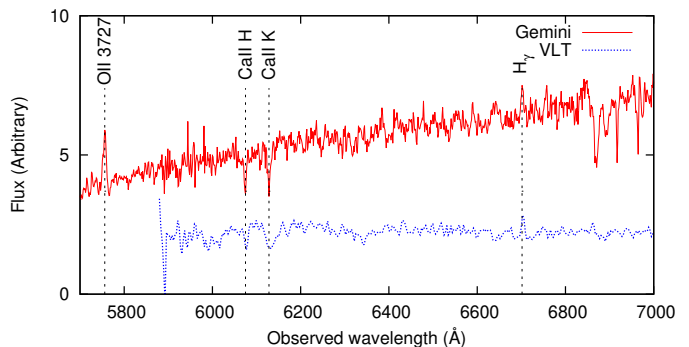


FIG. 2.— Gemini-South GMOS spectrum of GRB 090424 afterglow and the VLT FORS spectrum of its host galaxy.

TABLE 1
PROPERTIES OF GRB 081007 AND GRB 090424

Name	GRB 081007	GRB 090424
T_{90} (s)	8.0 (1)	48 ± 3 (2)
z	0.5295 ± 0.0001	0.544
E_{peak} (keV)	61 ± 15 (1)	236^{+127}_{-49} (3)
$E_{\gamma, \text{iso}}$ (erg)	$1.5^{+0.4}_{-0.3} \times 10^{51}$ (1)	$4.3^{+2.4}_{-1.4} \times 10^{52}$ (3)
Γ	~ 200	> 170
R_B	$\sim 10R_e^{-0.75}$	$> 10R_e^{-0.72}$
SN	SN 2008hw	No detection
R_{galaxy}	> 24.63	22.01 ± 0.12

REFERENCES. — (1) de Ugarte Postigo et al. (2011), (2) Sakamoto et al. (2009), (3) Sakamoto et al. (2011).

(Cannizzo et al. 2009). XRT and UVOT started observations 85 and 91 s after the trigger and detected the X-ray and optical afterglow (Cannizzo et al. 2009). Gemini-South took two 1200 s spectra, starting 11.7 hr after the burst, and found that GRB 090424 is at $z = 0.544$, similar to GRB 081007 (Chornock et al. 2009, see also figure 2).

The main properties of the two GRBs are summarized in Table 1. This work is structured as follows: in Section 2 we present the data. The discussion and interpretation of the observations are reported in Section 3. We summarize our results in Section 4.

2. OBSERVATIONS AND RESULTS

2.1. *The GRB 081007 and GRB 090424 afterglows*

Many robotic telescopes reacted to the trigger from GRB 081007. RAPTOR started observations detecting the optical counterpart after about 24 s in the R

band (Wren et al. 2008). Four of the 40 cm PROMPT telescopes at CTIO in Chile began observing after 41 s (West et al. 2008). The 60 cm Rapid Eye Mount (REM) on La Silla, Chile, started multi-band observations of GRB 081007 after 46 s in the R , H and K_s bands (Covino et al. 2008). The 2 m Faulkes Telescope North (FTN; Haleakala, Hawaii) started to observe GRB 081007 about 17 minutes after the *Swift* trigger in the B , V , R , and I bands (Smith et al. 2008). The 2 m Faulkes Telescope South (FTS; Siding Spring, Australia) observed the field of GRB 081007 from ~ 1.1 to ~ 4.2 days after the burst in the R and I bands. Between 2008 October 24 and 2009 January 3, FORS2 at the Very Large Telescope (VLT) was used to search for the SN associated with GRB 081007.

The 2 m Liverpool Telescope (LT; La Palma, Canary Islands, Spain) began observing the field of GRB 090424 at 21:29:47 UT (Guidorzi et al. 2009), ~ 7 hr after the burst. The optical counterpart was clearly detected in the r and i filters. Later observations were made by the FTN at 17.66 and 333.89 days after the trigger in the R filter only. Between 2009 May 1 and July 5, FORS2 at the VLT was also used to observe the GRB 090424 field for nine runs. Three years later, this field was observed again between 2012 May 1 to 3 with the 3.5m telescope at the Calar Alto Observatory.

Our dataset also includes *Swift*/UVOT data²⁶ and we have retrieved and analyzed public Gemini archival data²⁷ of GRB 081007 and GRB 090424, confirming results reported by Berger et al. (2008) and Chornock et al. (2009).

In this paper we analyzed all available photometric and spectroscopic data, following standard procedures: bias or dark removal, flat-field correction, astrometry for imaging frames and wavelength calibration for spectroscopy. Aperture photometry was calibrated by means of secondary standard stars in the field from the APASS catalog²⁸ or the Sloan Digital Sky Survey (SDSS) catalog²⁹ in the optical and the Two Micron All Sky Survey (2MASS) catalog³⁰ in the near-infrared (NIR). R and I band observations were calibrated by means of r' and i' secondary standard stars. Late-time photometric observations, since all secondary standard stars in the field were heavily saturated, were calibrated by means of standard star fields observed under photometric conditions. Spectroscopic observations were also calibrated by observations of suitable spectro-photometric standard stars.

We also collected data available from these GCN circulars: 8339 (Cobb 2008) for GRB 081007; 9224 (Yuan 2009), 9236 (Gorosabel et al. 2009), 9239 (Oksanen 2009), 9240 (Urata et al. 2009), 9245 (Olivares et al. 2009), 9246 (Nissinen & Hentunen 2009), 9248 (Im et al. 2009a), 9253 (Im et al. 2009b), 9278 (Roy et al. 2009), 9305 (Mao et al. 2009), 9313 (Cobb 2009), 9320 (Rumyantsev et al. 2009) for GRB 090424.

²⁶ The *Swift*/UVOT data are provided by the High Energy Astrophysics Science Archive Research Center (HEASARC).

²⁷ Gemini data are obtained at the Gemini Observatory, which is operated by the Association of Universities for Research in Astronomy.

²⁸ <http://www.aavso.org/apass>

²⁹ <http://www.sdss.org>

³⁰ <http://www.ipac.caltech.edu/2mass>

The photometric data are shown in Figures 3 and 4 and they are reported in the Appendix of the online journal (Tables 3 - 5). The (small) Galactic extinction, $E(B - V)$, of 0.016 and 0.025 mag (Schlegel et al. 1998) for GRB 081007 and GRB 090424, respectively, was taken properly into account in the analysis.

2.2. Discovery of a supernova accompanying GRB081007

A 2 hr spectrum of GRB 081007 was obtained with VLT equipped with FORS2 and the 300I grism on 2008 November 2 (Della Valle et al. 2008), about 26 days after the GRB trigger, and reduced following standard methods. After subtracting a starburst galaxy template (Sb1 template from Kinney et al. 1996), three broad bumps at about 4600, 5400, and 6400 Å emerge. These features are very similar to those exhibited by SN 1998bw (Patat et al. 2001) around maximum (see Figure 5), but the luminosity of the SN at maximum light is significantly lower than that of SN 1998bw at the same time, only about half as large as that of SN 1998bw (see Figure 6). This SN was designated SN 2008hw (Della Valle et al. 2008). Some similarities with other two broad-lined type Ic SNe, namely SN 1997ef (Mazzali et al. 2000) and SN 2004aw (Taubenberger et al. 2006) were also identified.

2.3. Host galaxy of GRB 090424

The optical counterpart of GRB 090424 shows no apparent variation from 18 days onwards, according to our FTN and VLT observations, no significant variation is found in Kann et al. (2010) either. This means the afterglow had faded below the host-galaxy brightness before this epoch. The VLT observed r and i band magnitudes of the host are $r = 22.07 \pm 0.12$ and $i = 21.82 \pm 0.12$, corresponding to a luminosity four times brighter than SN 1998bw at maximum light. An underlying SN akin to SN 1998bw would only have produced little additional brightening, at a level below the uncertainty in the galaxy luminosity. Additionally to the bright host galaxy, the afterglow suffers from significant host-frame extinction according to Kann et al. (2010); Schady et al. (2012) and Covino et al. (2013), which will further dim any SN component. This fact may explain the lack of detection of the SN component in the afterglow of GRB 090424 (see Figure 7).

The GRB 090424 host-galaxy spectrum was obtained with VLT-FORS2 and grism 300I on 2009 May 22, and with the Gran Telescopio Canarias (GTC) on 2013 April 8, about a month and 4 years after the high energy event respectively. These spectra were reduced following standard methods. The signal-to-noise ratio (S/N) of our VLT-FORS2 spectrum is $\sim 10 - 20$ in the blue part and goes down to 5-10 in the red part, the strong residual around 9400Å is due to telluric water vapor. Two absorption lines at 6077 and 6133 Å and emission lines at 6704, 7508, 7733, and 10135 Å are clearly detected, which are identified as Ca II K and H, H γ , H β , [O III] and H α at $z = 0.544$ (see Figure 8). The S/N of our GTC spectrum is $\sim 5 - 10$, it extends the VLT-FORS2 spectrum to the blue-ward, and an extra strong emission line at 5758 Å is detected, it is identified as [O II] at $z = 0.544$ (see Figure 8). We derived the fluxes for these lines first by remov-

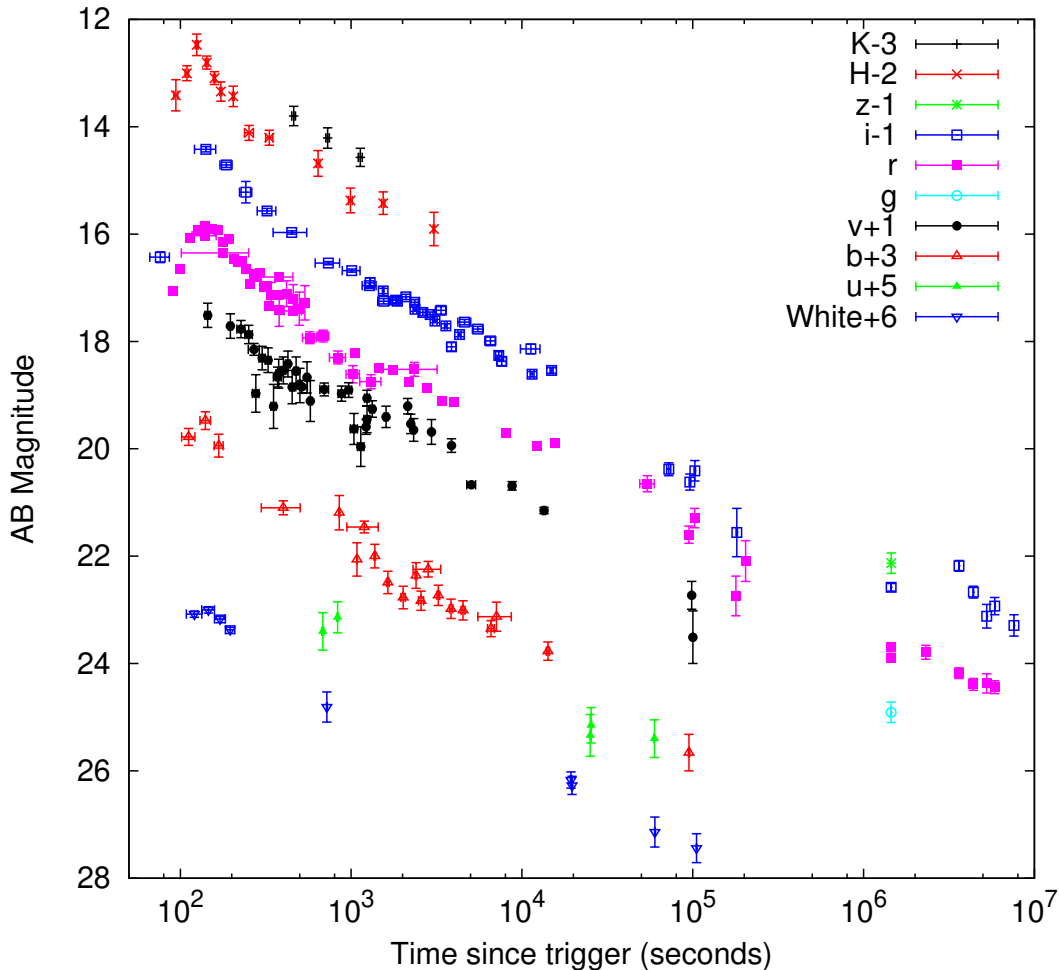


FIG. 3.— Optical/NIR observations of the GRB 081007 afterglow. Similar filters (e.g., Johnson R and SDSS r) are plotted with the same symbols for clarity in the figure. The data can be found in Tables 3 and 4 in the online material.

TABLE 2
SPECTRAL LINES OF THE GRB 090424 HOST GALAXY

Line	λ_{rest} Å	λ_{obs} Å	FWHM Å	F 10^{-18} cgs
[O II]	3727.09	5758.10	8.87 ± 1.16	82.25 ± 13.82
Ca II K	3934.78	6076.66	5.83 ± 1.84	-3.73 ± 1.59
Ca II H	3969.59	6132.57	16.81 ± 3.02	-11.01 ± 2.62
H γ	4341.68	6703.95	7.59 ± 0.44	7.14 ± 0.55
H β	4862.68	7508.30	7.94 ± 0.63	23.00 ± 2.41
[O III]	4960.30	7659.25	9.94 ± 1.27	7.06 ± 1.20
[O III]	5008.24	7733.10	9.90 ± 0.43	25.13 ± 1.45
H α	6564.61	10135.45	11.35 ± 0.48	151.64 ± 8.45
N II	6585.27	10164.24	8.33 ± 4.02	19.08 ± 12.15

NOTE. — The flux F is as observed, but the Galactic extinction has been taken into account for the analysis.

ing the background with a polynomial fit and then by modeling the lines with Gaussians. The resolution of our spectra does not justify a more sophisticated modeling. The results are summarized in Table 2.

3. INTERPRETATION AND IMPLICATION OF THE DATA

3.1. Interpreting the GRB 081007 afterglow

The most interesting feature of the early REM light curve of GRB 081007 is a bright peak in the H band data (see Figure 6). The light curve first rises as $t^{+3.0}$ and

peaks at approximately 130 s, then it decays very rapidly as $t^{-2.0}$ until about 300 s. Finally, there is a slower decay $\propto t^{-0.65}$. The RAPTOR, REM, and PROMPT r' data (see Figure 6), and PROMPT B and i' data (see Figure 3) also show a similar behavior, the three Ks -band points also follow an analogous decay but they are affected by large uncertainties and therefore we disregard them in our subsequent analysis of the afterglow.

The temporal behavior of the early-time optical afterglow is a powerful diagnostic of the circumburst medium density profile (Piran 1999), usually modeled as a power-law, $n \propto r^{-s}$, where n is the particle number density and r the distance from the burst progenitor. A homogeneous medium has $s = 0$, while $s = 2$ represents an environment shaped by a stellar wind from the GRB progenitor. In this scenario, the early t^{+3} optical afterglow rise could be due to the onset of either the forward shock from the outflow getting decelerated in the interstellar medium (ISM) or of the reverse shock emission if it is sub-relativistic (Rees & Mészáros 1992; Sari 1998; Sari & Piran 1999; Jin & Fan 2007). In both cases, however, a wind-shaped environment can be ruled out, since the optical afterglow rise cannot be faster than $t^{1/2}$ (Mészáros & Rees 1997; Mészáros et al. 1998; Chevalier & Li 2000; Jin & Fan 2007), because of the

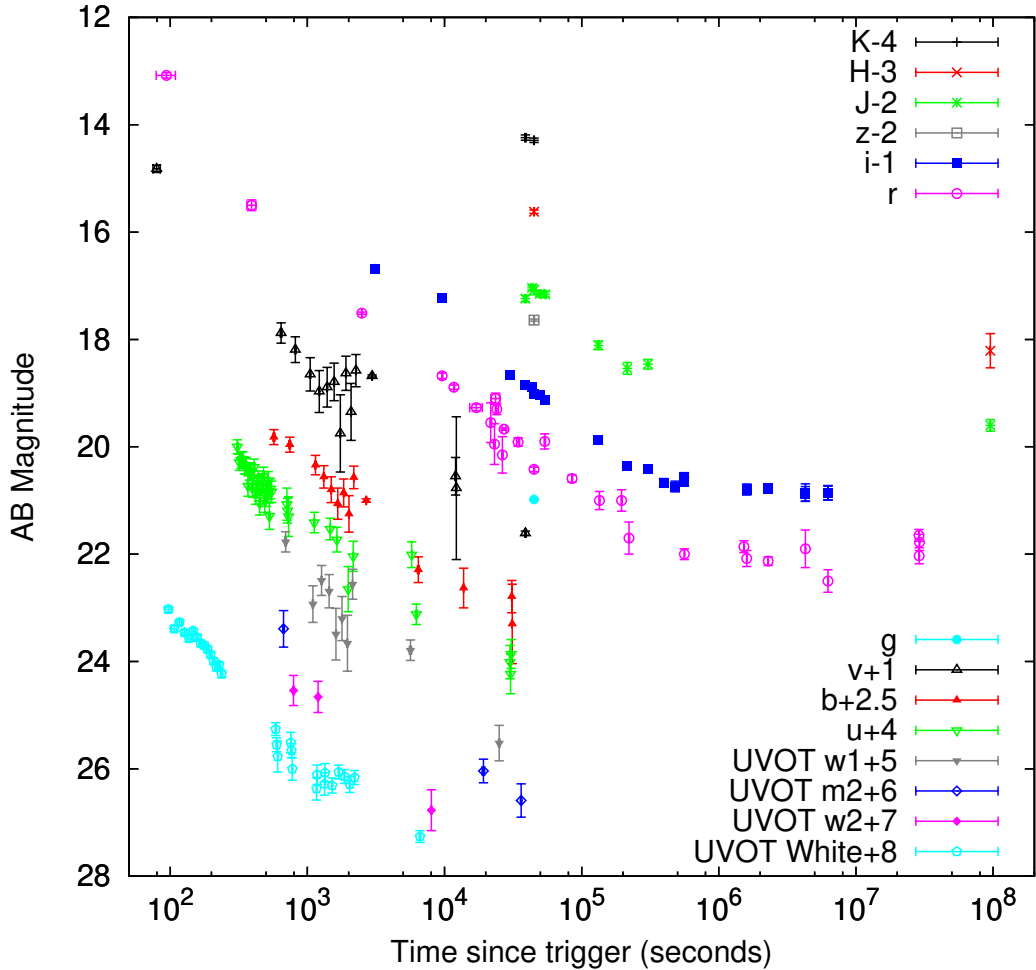


FIG. 4.— Optical/NIR observations of the GRB 090424 afterglow. Similar filters (e.g., Johnson R and SDSS r) are plotted with same the symbols for clarity in the figure. The data can be found in Table 5 in the online material.

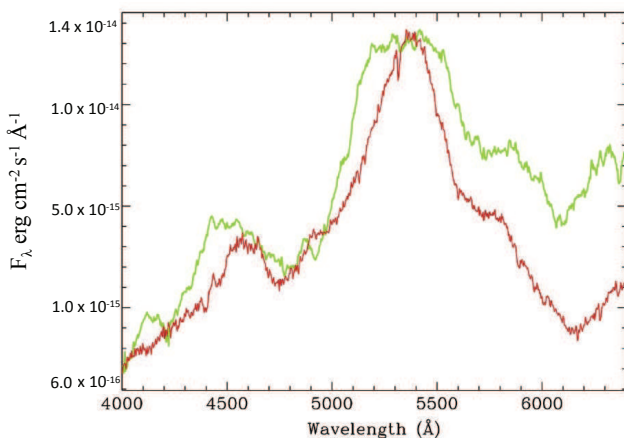


FIG. 5.— VLT-FORS2 spectrum of the optical counterpart of GRB 081007 taken on Nov 2, 2008, cleaned from telluric absorptions and sky lines and smoothed with a boxcar of 30 Å (green trace), compared with the spectrum of SN 1998bw close to maximum light (red trace, from Patat et al. 2001). The similarity suggests the presence of a supernova underlying GRB081007, dubbed SN 2008hw. The spectrum of SN 2008hw was rescaled to best match the features of SN1998bw.

rapidly decreasing circumburst density seen by the outflow.

The rapid optical decline ($\propto t^{-2}$) after the peak can only be interpreted in the context of reverse shock emission, such as the one observed in GRB 990123 (Akerlof et al. 1999; Sari & Piran 1999; Kobayashi 2000). Forward shock emission can decay so steeply only after a jet-break, which is unlikely the case at such early time. Therefore, the early t^{+3} rise is also due to the onset of the reverse shock emission from an outflow propagating in a constant density circumburst medium.

The *Swift*/XRT light curve of GRB 081007 can be divided into three power-law decay stages with indices -4.0 ± 0.4 , $-0.74^{+0.03}_{-0.05}$, and $-1.23^{+0.11}_{-0.10}$ (UK *Swift* Science Data Centre, Evans et al. 2009). The last two stages are similar to the simultaneous optical ones, which can be fitted by a $t^{-0.65}$ and a $t^{-1.25}$ decay, except for the last several observations, when the SN is already dominating the flux. The SN-dominated phase can be interpreted by the sum of a power-law afterglow, a SN template and an underlying host galaxy (see Figure 6). The initial sharp t^{-4} decay in X-rays suggests that this emission is the tail of the prompt emission (e.g., Zhang & Mészáros 2004).

The X-ray and optical data between 500 and 2×10^5

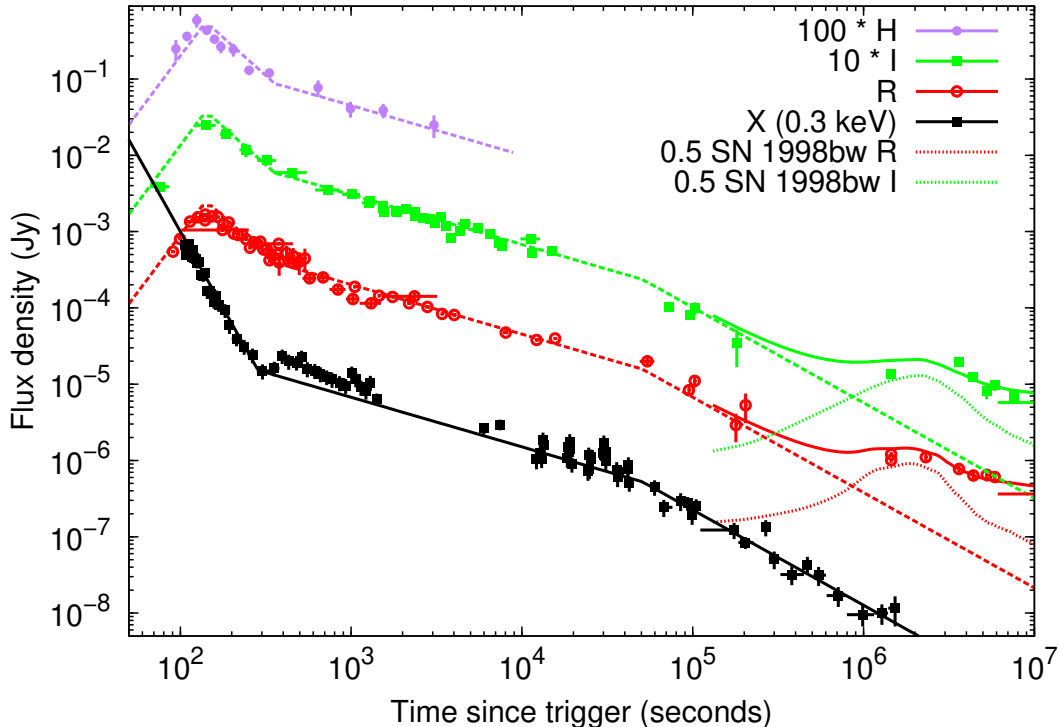


FIG. 6.— Fits to the GRB081007 afterglow observations. The broken power-law lines with slope indices 3, -2 , -0.65 , and -1.25 for the optical/NIR (long-dashed lines), and -4 , -0.65 , and -1.25 for the X-rays (black solid line) represent the afterglow light curves. The R and I -band late observations can be interpreted as the sum (red and green solid lines respectively) of the power-law afterglow, a SN template and a host-galaxy component, here the SN is 0.5 times as bright as SN 1998bw, reported at $z = 0.5295$, the host galaxy is $m_R = 25.0$ and $m_I = 24.5$ (short lines on the right). The SN template is also plotted for comparison (dotted line). The *Swift*/XRT X-ray light curve has been retrieved from the UK *Swift* Science Data Centre (Evans et al. 2009).

s exhibit pretty much the same decay slope (see Figure 6). The early shallow decline in both the X-ray and optical/NIR bands, roughly $t^{-0.65}$ can be interpreted as forward shock emission for a flat electron spectral index $p \approx 1.5$, while the late, roughly $t^{-1.25}$, decay may be due to the jet effect as long as the sideways expansion of the decelerating ejecta can be ignored (for which the light curve slope before and after the break would steepen by 0.75, close to what we observed). This interpretation is however inconsistent with the X-ray spectrum. The time-averaged photon spectral index of second X-ray epoch (between ~ 13 ks) *Swift*/XRT data is $2.10^{+0.15}_{-0.14}$ (UK *Swift* Science Data Centre, Evans et al. 2009), which suggests a normal electron spectral index $p \approx 2.2$. We thus interpret the $t^{-0.65}$ decay, too shallow compared to model predictions, as the emission of the forward shock with continued energy injection as $dE/dt \propto t^{-q}$ from the central engine, and the $t^{-1.25}$ decay as the end of injection. Following Zhang et al. (2006), it is straightforward to show that the afterglow decay index is $\alpha = [(2p-4) + (p+2)q]/4$, so the temporal index for an energy injection index $q = 0.5$ can reproduce the data, assuming that the optical band is above both the cooling frequency ν_c and the typical synchrotron radiation frequency ν_m of the forward shock. When both the cooling and synchrotron radiation frequency lie redward of the optical, a similar intrinsic spectral index of about -1.1 is expected in X-ray and optical bands (Zhang & Mészáros 2004), and is consistent with the

spectral energy distribution (SED) fit by Covino et al. (2013). For the energy injection from a spinning-down pulsar the early energy injection rate should have $q = 0$ (Dai & Lu 1998a), which is not consistent with what we observe. Therefore, a magnetized pulsar as a central engine cannot explain the observations.

3.2. Interpreting the GRB 090424 afterglow

GRB 090424 was also bright at early times (see Figure 4) as shown by UVOT observations, as well as R -band observations by TAOS and ROTSE-III (see Figure 7). The optical light curve was already decaying at the time of the first observations and the decay index was ≈ -1.5 , consistent with the prediction for the reverse shock emission. The optical and X-ray light curves can be well-fitted with a simple broken power-law. The indices of three optical slopes are -1.5 , -0.85 , and 0 , respectively. Assuming that the first phase is dominated by the reverse-shock component, the second phase is likely dominated by the forward shock emission that gradually overshone the fading reverse shock emission. At late times, the emission is dominated by the host galaxy, as shown by the constant luminosity. The best fit to the X-ray emission is four phases with decay indices $-1.29^{+0.06}_{-0.05}$, $-0.74^{+0.02}_{-0.03}$, -1.12 ± 0.02 , and $-1.42^{+0.18}_{-0.12}$, respectively (UK *Swift* Science Data Centre, Evans et al. 2009).

According to standard predictions of the fireball model in a wind-shaped environment, the X-ray light curve should be shallower than the optical light curve (e.g.,

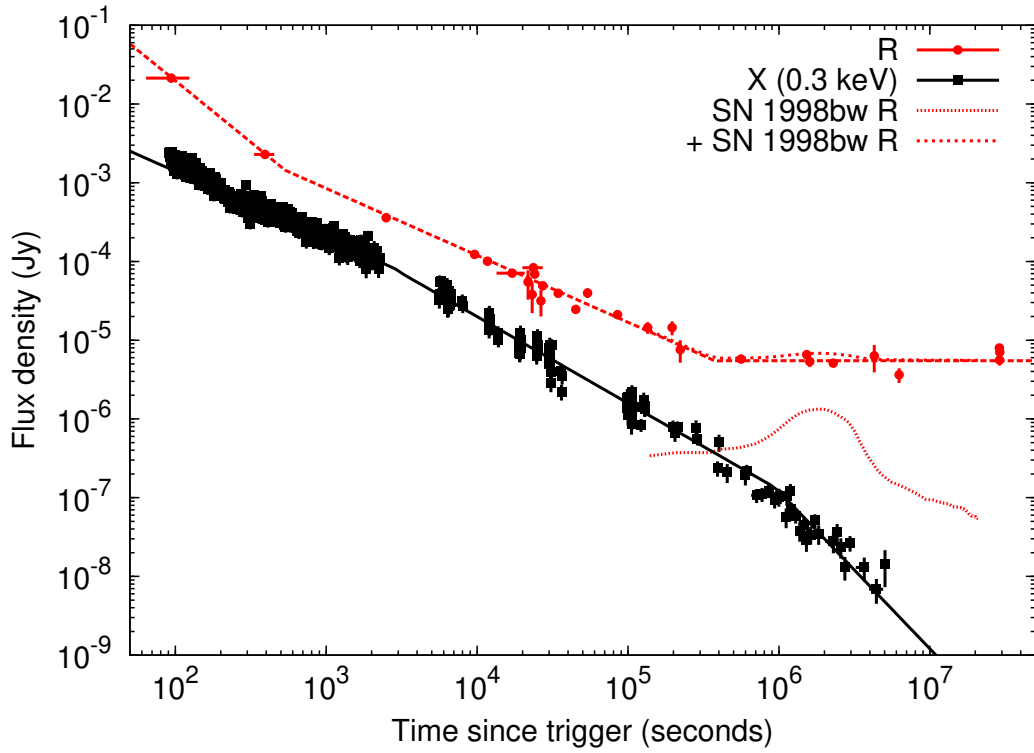


FIG. 7.— Simple broken power-law fits to the observations of the GRB090424 afterglow. The slope indices are -1.5 , -0.85 and 0 for the R band (long dashed line), -0.85 , -1.1 , and -2 for the X-rays (solid line). A smoothed light curve of SN 1998bw, shifted to $z = 0.544$, is plotted for comparison (dotted line). An underlying SN like SN 1998bw would contribute minimally to the total flux (short dashed line), below the uncertainty of the luminosity of the host galaxy. The X-ray light curve has been derived using the *Swift*/XRT data from the UK *Swift* Science Data Centre (Evans et al. 2009).

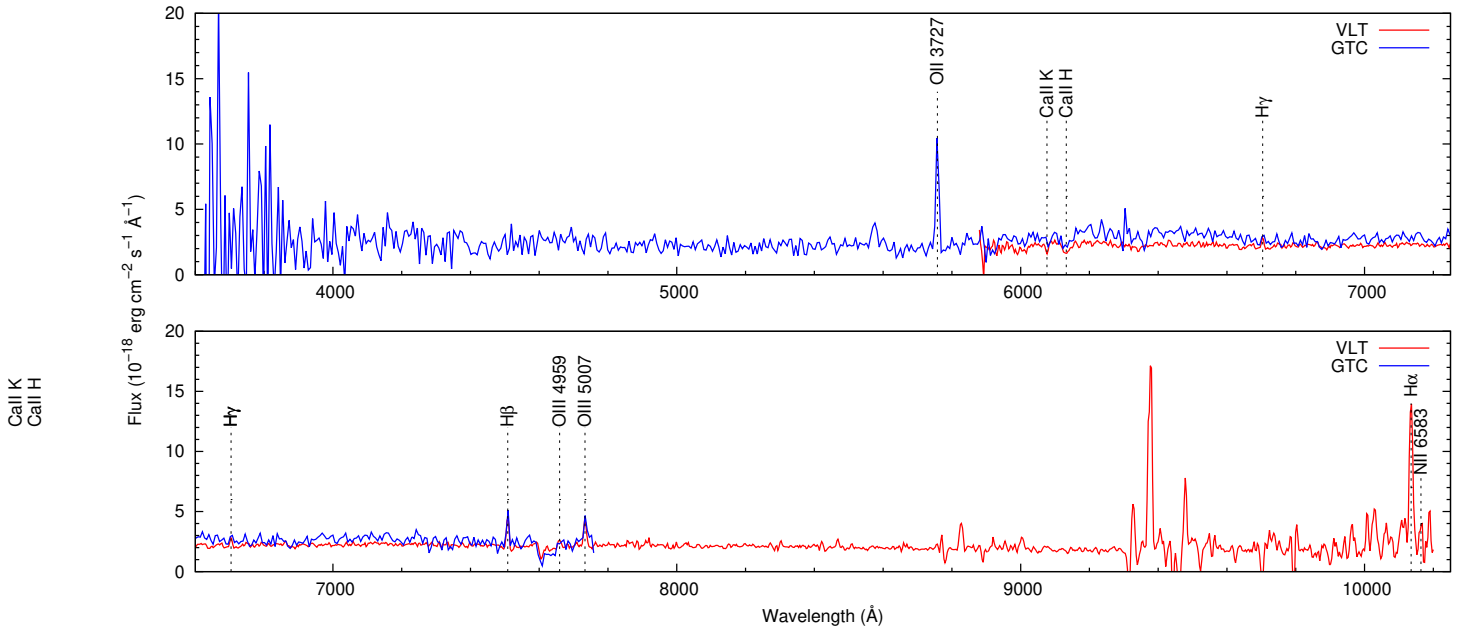


FIG. 8.— The VLT/FORS2 and the GTC spectra of the GRB090424 host galaxy in the observer frame.

Piran 1999; Jin et al. 2009), which is not the case for our data. The X-ray emission is likely due to the forward shock since, in most cases, the reverse-shock emission in the X-ray band is very weak and can be ignored (Fan & Wei 2005; Xue et al. 2009). We thus interpret the X-ray emission as being due to the forward shock. Between 3000 and 3×10^5 s, its decay index is steeper than the optical by a factor about 0.25, a spectral break between X-ray and optical is then required. This is also confirmed by the SED fits to the X-ray and optical observations by Schady et al. (2012) and Covino et al. (2013), a spectral break of 0.5 is required from X-ray to optical bands. With an ISM-like constant density medium the forward shock is expected to be in the slow cooling phase, i.e., the typical synchrotron frequency is below the cooling frequency ($\nu_m < \nu_c$). We find that $\nu_m < \nu_{\text{opt}} < \nu_c < \nu_X$, here ν_{opt} and ν_X represent the optical and X-ray bands of the observations. We also notice that around 3 ks, the decay of the X-ray light curve steepens by about 0.25 (the X-ray light curve before 3 ks can also be fitted with a single power law with decay index -0.88 , see UK *Swift* Science Data Centre, Evans et al. 2009), which is expected when the cooling frequency ν_c crosses the observational band ($\sim 7 \times 10^{16}$ Hz, or about 0.3 keV). Applying standard relations (e.g., Zhang & Mészáros 2004), this change can be interpreted as $-0.85 (3[p - 1]/4)$ to $-1.1 ([3p - 2]/4)$, with the electron power-law distribution index being $p = 2.13$. Given the time evolution of the cooling frequency, $\nu_c \propto t^{-1/2}$, it will have crossed the *R* band ($\approx 4.2 \times 10^{14}$ Hz) at about 8×10^7 s. Finally, the last steepening from -1.1 to -1.4 is likely due to a jet break. Fixing the final stage of X-ray decay to -2 , the break is occurring at $\sim 10^6$ s.

From the break time, the jet opening angle can be estimated as explained e.g., by (Sari et al. 1999):

$$\theta_j = 0.161 \left(\frac{t_{\text{jet,day}}}{1+z} \right)^{3/8} \left(\frac{n_0 \eta}{E_{\gamma,\text{iso},52}} \right)^{1/8} \text{ rad}, \quad (1)$$

where $E_{\gamma,\text{iso}}$ is the isotropic-equivalent energy of the prompt gamma-ray emission, n_0 is the number density of the medium in cm^{-3} and η is the GRB efficiency, which we take to be ~ 1 and ~ 0.2 respectively. Here and throughout this text, the convention $Q_x = Q/10^x$ has been adopted in cgs units except for some special notations. Therefore for GRB 090424, with $t_{\text{jet,day}} \sim 12$, we have $\theta_j \sim 14^\circ$; while for GRB 081007, with $t_{\text{jet,day}} > 12$ we have $\theta_j > 20^\circ$.

3.3. Estimating the Lorentz factor of the outflows

For both GRB 081007 and GRB 090424 the prompt emission duration T is shorter than the outflow deceleration time t_{dec} . In this case the reverse shock crossing time t_\times is comparable to the forward-shock deceleration time (for a review see Mészáros 2006), that is:

$$t_\times = t_{\text{dec}} = 10 \left(\frac{E_{k,53}}{n_0} \right)^{1/3} \Gamma_{2.5}^{-8/3} \text{ s}, \quad (2)$$

where $E_k = E_{\gamma,\text{iso}}/\eta$. The outflow Lorentz factor in turn can be estimated as (e.g., Molinari et al. 2007):

$$\Gamma \sim 160 \left[\frac{E_{\gamma,\text{iso},53}(1+z)^3}{n_{0.2} n_0 t_{\text{dec},2}^3} \right]^{1/8}. \quad (3)$$

For GRB 081007, $z = 0.5295$, $E_{\gamma,\text{iso}} \sim 1.5 \times 10^{51}$ erg, and $t_{\text{dec}} \sim 130$ s, yielding $\Gamma \sim 200(\eta_{0.2} n_0)^{1/8}$. For GRB 090424, $z = 0.544$, $E_{\gamma,\text{iso}} \sim 4.3 \times 10^{52}$ erg, and $t_{\text{dec}} \leq 100$ s, yielding $\Gamma \geq 170(\eta_{0.2} n_0)^{1/8}$.

In both cases the initial GRB outflows are relativistic, consistent with what has been found in previous works (e.g., Molinari et al. 2007; Sari & Piran 1999; Xue et al. 2009).

3.4. Constraining the magnetization of the outflows

Based on the relative strength of forward- and reverse-shock emission, early GRB afterglows can be classified into three categories (Jin & Fan 2007; Zhang et al. 2003): Type I, showing both peaks of the forward- and reverse-shock emission; Type II, where the strong reverse-shock emission outshines the peak emission of the forward shock; Type III, where the reverse-shock emission is absent. The difference between these three types is attributed to the very different magnetization degrees of the outflow (see Jin & Fan 2007, for more detail). Note that the classification in types I, II and III has here a different meaning than in Zhang et al. (2007). For GRB 081007 and GRB 090424, bright optical peaks from the reverse-shock emission have been identified, and no forward-shock optical peak emission can be detected, therefore, they are both Type II afterglows, for which the reverse-shock region is expected to be mildly magnetized, as shown in previous works (e.g., Fan et al. 2002; Zhang et al. 2003; Fan et al. 2005b). In case the observer frequency lies above $\nu_m(t_\times)$ but below $\nu_c(t_\times)$, the ratio between the reverse-shock optical emission at its crossing time (F_{obs}^r) and the forward-shock optical peak emission can be estimated by (as in Jin & Fan 2007):

$$\frac{F_{\text{obs}}^r(t_\times)}{F_{\text{obs}}(t_p)} = 0.08 R_e^{p-1} R_B^{(p+1)/2} \left(\frac{t_p}{t_\times} \right)^{3(p-1)/4}, \quad (4)$$

where $R_B \equiv \varepsilon_B^r/\varepsilon_B$, ε_B^r (ε_B) is the fraction of the reverse (forward) shock energy given to the magnetic field, $R_e \equiv \varepsilon_e^r/\varepsilon_e$, and ε_e^r (ε_e) is the fraction of the reverse (forward) shock energy given to the electrons.

For GRB 081007, we have $F_{\text{obs}}^r(t_\times) \sim 0.002$ Jy and $t_\times \sim 130$ s. The underlying forward-shock emission peaks (t_p) between t_\times and ~ 300 s (when it outshines the reverse-shock emission), and the peak flux is ~ 0.0005 Jy. For $p \sim 2.2$ we have $R_B \sim 10R_e^{-0.75}$.

For GRB 090424, if we consider the first TAOS *R*-band observation (Urata et al. 2009) as the reverse-shock peak, then the flux is 0.02 Jy at 90 s. The forward-shock emission dominates the afterglow at 400 s, when the corresponding flux is 0.002 Jy. Taking $p \sim 2.13$ and $t_p \sim 400$ s, we have $R_B \sim 10R_e^{-0.72}$. It is possible that the reverse-shock peak is earlier and the flux is higher or the forward-shock emission peak is earlier: so the derived R_B is only a lower limit.

The numerical fit to the multi-wavelength afterglow data of GRBs usually gives $\varepsilon_e \sim$ a few $\times 0.1$ (e.g., Panaitescu & Kumar 2001). Since $\varepsilon_e^r < 1$, we have $R_e \leq$ a few and then $R_B >$ a few. In other words the reverse-shock regions are mildly magnetized. One straightforward speculation from this is that the optical flash photons should have a moderate linear polarization degree, as has been detected in GRB 090102 (Steele et al. 2009).

3.5. Linking SN 2008hw with homogenous circumburst medium

GRB 081007 is an event showing an optical onset and a clearly identified SN associated with it. As discussed in Sect. 3.1, afterglow data allow us to constrain the density profile of the circumburst medium, while the occurrence of a SN confirms that the progenitor is a massive star. The afterglow analysis suggests, as it is indeed fairly common for GRBs (e.g., Schulze et al. 2011), that the outflow powering GRB 081007 was propagating in a constant density medium. On the other hand, a massive stellar progenitor is expected, during its final stages of evolution, to eject a dense wind shaping the surrounding density profile, in possible contradiction with results based on afterglow analysis. In the past, GRBs with bright optical flashes and an associated SNe were GRB 021211/SN2002lt (Fox et al. 2003; Li et al. 2003; Della Valle et al. 2003), GRB 050525A/SN2005nc (Shao & Dai 2005; Della Valle et al. 2006; Blustin et al. 2006) and GRB 080319B (Racusin et al. 2008; Bloom et al. 2009; Tanvir et al. 2010).

It is widely speculated that strong episodes of mass loss occur before the death of massive stars (e.g., Pastorello et al. 2007), which is why GRBs are expected to explode in wind-shaped media (Dai & Lu 1998b; Chevalier & Li 2000; Ofek et al. 2013). However, this does not seem to be the case for GRB 081007/SN 2008hw, as we have shown in this work. A similar situation was encountered with other nearby GRB/XRF associated with energetic and luminous SNe: GRB 030329/SN2003dh, XRF 060218/SN2006aj (e.g., Fan 2008), although both the gamma-ray signatures and SNe were quite different (Stanek et al. 2003; Hjorth et al. 2006; Mazzali et al. 2003; Campana et al. 2006; Pian et al. 2006; Mazzali et al. 2006). Also for GRB 090618, at a similar redshift $z = 0.54$, observations seem to favor a homogeneous ISM environment over a wind environment (Page et al. 2011; Cano et al. 2011).

The GRB 081007 data suggest that the expansion and interaction of SN shells is occurring in a medium with density profile more typical of a homogenous ($\sim r^0$) ISM rather than a stellar wind ($\propto r^{-2}$) medium. One possible explanation for this inconsistency is that mass loss occurring during the final stages of the life of the massive progenitor proceeds “discretely” through sudden ejection of blobs of matter (e.g., Pastorello et al. 2007) rather than “smoothly” with a continuous, constant rate. If the time between blob-ejection is long enough, then there is time to redistribute matter inside the circumstellar medium and to make it sufficiently homogeneous. Afterglow data, extending up to 10 days after the trigger in the observer frame, can be used to set a lower limit on the time interval that separates pulses. Since the external shock propagates with almost luminal velocity, the distance covered by the plasma is $\delta ct/(1+z)$, where $\delta = 1/\Gamma[1 - \cos(\theta)]$ is the Doppler factor. If we assume an average value $\langle \Gamma \rangle \sim 10$ during this time, it will take > 100 years for a wind moving at 1000 km s^{-1} to cover this distance. This first order computation roughly estimates the time needed for the medium surrounding the progenitor to change the trend of the density profile from $\propto r^{-2}$ to $\propto r^0$. This time can be used to constrain models of

mass ejection in the late phases of massive-star evolution, which is still poorly understood.

3.6. Origin of the “single-pulse” prompt emission of GRB 081007

The prompt emission of GRB 081007 can be modeled as a single pulse (Markwardt et al. 2008; Bissaldi et al. 2008). In some nearby under-luminous bursts such as GRB 980425 (Pian et al. 2000), XRF 060218 (Campana et al. 2006) and XRF 100316D (Starling et al. 2011), the prompt emission was also characterized by a single pulse. The physical origin of the prompt emission is still widely debated, with theories also including the shock breakout of the SN explosion and the external forward-shock emission. For GRB 081007, these two models are actually disfavored. The inferred $\Gamma \sim 200$ is so high that the “shock breakout” radius would be as large as $\sim 2\Gamma^2 cT_{90}/(1+z) \sim 10^{16} \text{ cm}$, which is too large. In the case of the external-shock model, a single-pulse-like prompt emission is in principle possible and the duration of the prompt emission would trace the deceleration of the outflow. However, the well-delineated peak of the optical afterglow, likely marking the deceleration of the outflow at a time $\sim 130 \text{ s}$, renders the interpretation of the short-lived prompt emission as the external shock(s) unlikely.

Below we discuss the possibility that GRB 081007 was powered by the magnetic energy dissipation of a Poynting-flux dominated outflow. Such a model is partly motivated by the mild magnetization inferred from the optical afterglow data.

Following Usov (1994), the radius at which the MHD condition breaks down can be estimated following Fan et al. (2005a)

$$r_{\text{MHD}} \sim 2 \times 10^{16} L_{50}^{1/2} \sigma_1^{-1} t_{v,m,-3} \Gamma_2^{-1} \text{ cm}, \quad (5)$$

where σ_1 is the ratio of the magnetic energy flux to the particle energy flux, L is the total luminosity of the outflow, and $t_{v,m}$ is the minimum variability timescale of the central engine. Beyond this radius, significant magnetic dissipation processes are expected to happen which convert energy into radiation. The radiation timescale is (Gao & Fan 2006)

$$\tau \sim \frac{(1+z)r_{\text{MHD}}}{2\Gamma^2 c} = 33 \text{ s} (1+z) L_{50}^{1/2} \sigma_1^{-1} t_{v,m,-3} \Gamma_2^{-3}, \quad (6)$$

and the corresponding synchrotron radiation frequency can be estimated as (Fan et al. 2005a; Gao & Fan 2006)

$$\nu_{m,\text{MHD}} \sim 6 \times 10^{16} \sigma_1^3 C_p^2 \Gamma_2 t_{v,m,-3} (1+z)^{-1} \text{ Hz}, \quad (7)$$

where $C_p \equiv (\varepsilon_e/0.5)[13(p-2)]/[3(p-1)]$, and ε_e is the fraction of the dissipated comoving magnetic-field energy converted to the comoving kinetic energy of the electrons. Adopting $L \sim 10^{51} \text{ erg s}^{-1}$, $\sigma \sim 50$ and $\Gamma \sim 200$, the prompt emission data of GRB 081007 (including the duration as well as the peak energy) can be well reproduced.

After the identification of a distinct thermal radiation component in GRB 090902B (e.g., Ryde et al. 2010; Zhang et al. 2011), the photospheric radiation model has attracted wide attention. In such a scenario, the prompt gamma-rays are produced by the significantly modified quasi-thermal radiation from the photosphere

of the outflow or from sites with an optical depth of ~ 10 (Beloborodov 2013, and references therein). For GRB 081007, such an origin can not be ruled out. With future γ -ray polarimetry data (see Götz et al. 2009; Yonetoku et al. 2011, for preliminary results) we may be able to distinguish between the global-magnetic-energy-dissipation model and the photospheric-radiation model, since the former usually predicts a moderate or high linear polarization while the latter usually does not. One exception is that in a specific photosphere model moderate linear polarization is possible if our line of sight happens to be at the edge of the ejecta (Fan 2009).

3.7. Host galaxy parameters

The apparent magnitudes of host galaxy of GRB 090424 are $r = 22.07 \pm 0.12$ and $i = 21.82 \pm 0.12$, so the absolute magnitudes are approximately $M_B = -20.47 \pm 0.12$ and $M_V = -20.69 \pm 0.12$, considering the Galactic extinction $E(B - V) = 0.025$. These figures are close to the values for our Galaxy, and are brighter than for most GRB hosts (see e.g., Hjorth et al. 2012).

The metallicity of a galaxy can be derived from the ratio of different emission lines in its spectrum. Several methods have been studied and adopted (for a recent review, see Kewley & Ellison 2008). In our case, we used the N2 and O3N2 indices, as recalibrated by Pettini & Pagel (2004). We find a metallicity $12 + \log(\text{O}/\text{H})$ of about 8.39 and 8.43 using the N2 and O3N2 methods, respectively. These two methods are also weakly affected by intrinsic or Galactic extinction.

The observed fluxes of the $\text{H}\alpha$ and $\text{H}\beta$ emission lines are 151.64 ± 8.45 and $20.49 \pm 3.04 \times 10^{-18} \text{ erg s}^{-1} \text{ cm}^{-2}$. To estimate the SFR from the $\text{H}\alpha$ or $\text{H}\beta$ line, we followed the relations used in Savaglio et al. (2009): $\text{SFR}_{\text{H}\alpha} = 4.39 \times 10^{-42} L_{\text{H}\alpha} M_{\odot} \text{ yr}^{-1}$ and $\text{SFR}_{\text{H}\beta} = 12.6 \times 10^{-42} L_{\text{H}\beta} M_{\odot} \text{ yr}^{-1}$. Correcting for Galactic extinction, the lower limit (since the host galaxy extinction is not corrected) of SFR is $\text{SFR}_{\text{H}\alpha} = 0.80 M_{\odot} \text{ yr}^{-1}$ or $\text{SFR}_{\text{H}\beta} = 0.32 M_{\odot} \text{ yr}^{-1}$.

4. SUMMARY

In this paper we have presented and interpreted multi-wavelength observations of GRB 081007 and GRB 090424, and we summarize here the results.

i) The early stages of both afterglows are characterized by a bright optical/NIR component, which we interpret as the reverse-shock emission.

ii) The late-time afterglow of GRB 081007 is dominated by a SN component (SN 2008hw) similar to SN 1998bw near maximum light. The presence of a SN associated with the GRB clearly suggests that this burst originated from a massive star that should have shaped its circumburst environment with wind. On the other hand, the afterglow data can only be interpreted assuming a surrounding ISM-like medium, characterized by a constant density profile. A process to make the circumburst medium around the progenitor star homogeneous has likely been effective.

iii) The entire set of the afterglow data of GRB 081007 can be interpreted within the forward- and reverse-shock model, consider a long-lasting energy injection following the law $dE/dt \propto t^{-0.5}$.

iv) The initial Lorentz factor of GRB 081007 outflow is estimated by the afterglow data to be $\Gamma \sim 200$, which makes the interpretation of its single-pulse prompt emission in terms of both external forward shock and shock breakout unlikely. The identification of a reverse-shock emission component peaking at ~ 130 s after trigger rules out the possibility that the short-lived prompt emission was due to external-shock emission. The absence of the peak of forward-shock optical emission strongly suggests that the reverse-shock regions should be mildly magnetized. We therefore suggest that the prompt emission, characterized by a single pulse, may be due to the magnetic energy dissipation of a Poynting-flux dominated outflow or to a dissipative photosphere.

v) For GRB 090424, we set a lower limit on the initial Lorentz factor of the outflow of $\Gamma > 170$. Unlike GRB 081007, we did not detect the SN component in the afterglow, likely due to the considerably bright host galaxy, roughly comparable to the Milky Way. The bright initial optical/NIR afterglow has also been attributed to emission from a mildly-magnetized reverse shock. The late time X-ray and optical data are consistent with the forward-shock model and the surrounding medium is also found to be ISM-like.

All these results demonstrate that multi-band afterglow data, in particular with very early observations, are a necessary and valuable tool to better understand GRB physics. Significant progress is expected in the near future as more data will be collected.

ACKNOWLEDGMENTS

We acknowledge the support from the ASI grants I/011/07/0 and I/088/06/0, the INAF PRIN 2009 and 2011, and the MIUR PRIN 2009ERC3HT. We thank the Paranal Science Operations staff, and in particular T. Rivinius, P. Lynam, S. Brilliant, F.J. Selman, T. Szeifert, L. Schmidtobreick, A. Smette, A. Ahumada, K. O'Brien, C. Ledoux for effectively carrying out our service-mode observations. We wish to acknowledge the anonymous referee who has significantly improved the presentation and the discussion of the data. The Dark Cosmology Centre is funded by the D NRF. J.P.U.F. acknowledges support from the ERC-StG grant EGGs-278202. The RAPTOR project is supported by the DOE sponsored LDRD program at LANL. The Liverpool Telescope is operated by Liverpool John Moores University at the Observatorio del Roque de los Muchachos of the Instituto de Astrofísica de Canarias. The Faulkes Telescopes are owned by Las Cumbres Observatory. CGM acknowledges support from the Royal Society. Data collected with the Gran Telescopio Canarias (GTC), installed in the Spanish Observatorio del Roque de los Muchachos of the Instituto de Astrofísica de Canarias, on the island of La Palma. Based on observations collected with the 3.5m telescope of the German-Spanish Astronomical Centre, Calar Alto, Spain, operated jointly by the Max-Planck-Institut für Astronomie (MPIA), Heidelberg, and the Spanish National Commission for Astronomy. This study was carried out in the framework of the Unidad Asociada IAA-CSIC at the group of planetary science of ETSI-UPV/EHU and supported by the Ikerbasque Foundation for Science. The research of J.G., A.J.C.T and R.S.R. is supported by the Spanish programmes AYA2008-03467/ESP, AYA2012-39727-C03-01

and AYA2009-14000-C03-01. Z.P.J. thanks Dr. Yi-Zhong Fan for stimulating discussion. Z.P.J. was sup-

ported by the National Natural Science Foundation of China under the grants 11073057 and 11103084.

REFERENCES

- Akerlof, C., Balsano, R., Barthelmy, S., et al. 1999, *Nature*, 398, 400
- Baumgartner, W. H., Cummings, J. R., Evans, P. A., et al. 2008, *GCN*, 8330
- Beloborodov, A. M. 2013, *ApJ*, 764, 157
- Berger, E., Chornock, R., Holmes, T. R., et al. 2011, *ApJ*, 743, 204
- Berger, E., Fox, D. B., Cucchiara, A., & Cenko, S. B. 2008, *GCN*, 8335
- Bissaldi, E., McBreen, S., & Connaughton, V. 2008, *GCN*, 8369
- Bloom, J. S., Perley, D. A., Li, W., et al. 2009, *ApJ*, 691, 723
- Blustin, A. J., Band, D., Barthelmy, S., et al. 2006, *ApJ*, 637, 901
- Campana, S., Mangano, V., Blustin, A. J., et al. 2006, *Nature*, 442, 1008
- Cannizzo, J. K., Barthelmy, S. D., Beardmore, A. P., et al. 2009, *GCN*, 9223
- Cano, Z., Bersier, D., Guidorzi, C., et al. 2011, *ApJ*, 740, 41
- Chevalier, R. A., & Li, Z. Y. 2000, *ApJ*, 536, 195
- Chornock, R., Perley, D. A., Cenko, S. B., & Bloom, J. S. 2009, *GCN*, 9243
- Cobb, B. E. 2008, *GCN*, 8339
- Cobb, B. E. 2009, *GCN*, 9313
- Colgate, S. A. 1968, *CaJPh*, 46, 476
- Covino, S., Antonelli, L. A., Calzoletti, L., et al. 2008, *GCN*, 8331
- Covino, S., Melandri, A., Salvaterra, R., et al. 2013, *MNRAS*, 432, 1231
- Dai, Z. G., & Lu, T. 1998a, *A&A*, 333, L87
- Dai, Z. G., & Lu, T. 1998b, *MNRAS*, 298, 87
- de Ugarte Postigo, A., Horváth, I., Veres, P., et al. 2011, *A&A*, 525, 109
- Della Valle, M. 2011, *IJMPD*, 20, 1745
- Della Valle, M., Benetti, S., Mazzali, P., et al. 2008, *CBET*, 1602
- Della Valle, M., Malesani, D., Benetti, S., et al. 2003, *A&A*, 406, L33
- Della Valle, M., Malesani, D., Bloom, J. S., et al. 2006, *ApJ*, 642, L103
- Evans, P. A., Beardmore, A. P., Page, K. L., et al. 2009, *MNRAS*, 397, 1177
- Fan, Y. Z. 2008, *MNRAS*, 389, 1306
- Fan, Y. Z. 2009, *MNRAS*, 397, 1539
- Fan, Y. Z., Dai, Z. G., Huang, Y. F., & Lu, T. 2002, *ChJAA*, 2, 449
- Fan, Y. Z., & Wei, D. M. 2005, *MNRAS*, 364, L42
- Fan, Y. Z., Zhang, B., & Proga, D. 2005a, *ApJ*, 635, L129
- Fan, Y. Z., Zhang, B., & Wei, D. M. 2005b, *ApJ*, 628, L25
- Filgas, R., Greiner, J., Schady, P., et al. 2011, *A&A*, 535, A57
- Fox, D. W., Price, P. A., Soderberg, A. M., et al. 2003, *ApJ*, 586, L5
- Galama, T. J., Vreeswijk, P. M., van Paradijs, J., et al. 1998, *Nature*, 395, 670
- Gao, W. H., & Fan, Y. Z. 2006, *ChJAA*, 6, 513
- Gehrels, N., Chincarini, G., Giommi, P., et al. 2004, *ApJ*, 611, 1005
- Ghirlanda, G., Ghisellini, G., Salvaterra, R., et al. 2013, *MNRAS*, 428, 1410
- Gorosabel, J., Kubanek, P., Jelinek, M., de Ugarte Postigo, A., & Aceituno, J. 2009, *GCN*, 9236
- Guetta, D., & Della Valle, M. 2007 *ApJ*, 657, L73
- Guidorzi, C., Bersier, D., & Tanvir, N. 2009, *GCN*, 9238
- Götz, D., Laurent, P., Lebrun, F., Daigne, F. & Bošnjak, Ž. 2009, *ApJ*, 695, L208
- Hjorth, J., & Bloom, J. 2012, in *Gamma-Ray Bursts*, ed. C. Kouveliotou, R. A. M. J. Wijers & S. Woosley (Cambridge Astrophysics Series 51; Cambridge: Cambridge Univ. Press), chap. 9
- Hjorth, J., Levan, A., Tanvir, N., et al. 2006, *The Messenger*, 126, 16
- Hjorth, J., Malesani, D., Jakobsson, P., et al. 2012, *ApJ*, 756, 187
- Hjorth, J., Sollerman, J., Möller, P., et al. 2003, *Nature*, 423, 847
- Im, M., Park, W., Jeon, Y. et al. 2009a, *GCN*, 9248
- Im, M., Park, W., Jeon, Y. et al. 2009b, *GCN*, 9253
- Jin, Z. P., & Fan, Y. Z. 2007, *MNRAS*, 378, 1043
- Jin, Z. P., Xu, D., Covino, S., et al. 2009, *MNRAS*, 400, 1829
- Li, W. D., Filippenko, A. V., & Chornock, R., Jha, S. 2003, *ApJ*, 586, L9
- Kann, D.A., Klose, S., Zhang, B., et al. 2010, *ApJ*, 720, 1513
- Kewley, L. J., & Ellison, S. L. 2008, *ApJ*, 681, 1183
- Kinney, A. L., Calzetti, D., Bohlin, R. C., et al. 1996, *ApJ*, 467, 38
- Kobayashi, S. 2000, *ApJ*, 545, 807
- Malesani, D., Tagliaferri, G., Chincarini, G., et al. 2004, *ApJ*, 609, L5
- Mao, J., Cha, G., & Bai, J. 2009, *GCN*, 9305
- Markwardt, C. M., Barthelmy, S. D., Baumgartner, W. H., et al. 2008, *GCN*, 8338
- Mazzali, P. A.; Deng, J., Nomoto, K., et al. 2006, *Nature*, 442, 1018
- Mazzali, P. A., Deng, J., Tominaga, N., et al. 2003, *ApJ*, 599, L95
- Mazzali, P. A., Iwamoto, K., & Nomoto, K. 2000, *ApJ*, 545, 407
- Mészáros, P. 2006, *RPPh*, 69, 2259
- Mészáros, P., & Rees, M. J. 1997, *ApJ*, 476, 232
- Mészáros, P., Rees, M. J., & Wijers, R. A. M. J. 1998, *ApJ*, 499, 301
- Molinari, E., Vergani, S. D., Malesani, D., et al. 2007, *A&A*, 469, L13
- Nissinen, M., & Hentunen, V. 2009, *GCN*, 9246
- Ofek, E.O., Sullivan, M., Cenko, S. B., et al. 2013, *Nature*, 494, 65
- Oksanen, A. 2009, *GCN*, 9239
- Olivares, F., Kupcu Yoldas, A., Greiner, J., & Yoldas, A. 2009, *GCN*, 9245
- Page, K. L., Starling, R. L. C., Fitzpatrick, G., et al. 2011, *MNRAS*, 416, 2078
- Panaitescu, A., & Kumar, P. 2001, *ApJ*, 554, 667
- Pastorello, A., Smartt, S. J., Mattila, S., et al. 2007, *Nature*, 447, 829
- Patat F., Cappellaro, E., Danziger, J., et al. 2001, *ApJ*, 555, 900
- Pettini, M., & Pagel, B. E. J. 2004, *MNRAS*, 348, L59
- Pian E., Amati, L., Antonelli, L. A., et al. 2000, *ApJ*, 536, 778
- Pian E., Mazzali, P. A., Masetti, N., et al. 2006, *Nature*, 442, 1011
- Piran T. 1999, *PhR*, 314, 575
- Racusin, J. L., Karpov, S. V., Sokolowski, M., et al. 2008, *Nature*, 455, 183
- Rees, M. J., & Mészáros, P. 1992, *MNRAS*, 258, 41
- Roy, R., Kumar, B., Pandey, S. B., & Kumar, B. 2009, *GCN*, 9278
- Ryde, F., Axelsson, M., Zhang, B. B., et al. 2009, 2010, *ApJ*, 709, L172
- Rumyantsev, V., Antoniuk, K., & Pozanenko, A. 2009, *GCN*, 9320
- Sakamoto, T., Barthelmy, S. D., Baumgartner, W. H., et al. 2009, *GCN*, 9231
- Sakamoto, T., Barthelmy, S. D., Baumgartner, W. H., et al. 2011, *ApJS*, 195, 2
- Sari, R. 1998, *ApJ*, 494, L49
- Sari, R., & Piran, T. 1999, *ApJ*, 517, L109
- Sari, R., Piran, T., & Halpern, J. P. 1999, *ApJ*, 524, L43
- Savaglio, S., Glazebrook, K., & Le Borgne, D. 2009, *ApJ*, 691, 182
- Schady, P., Dwelly, T., Page, M. J., et al. 2012, *A&A*, 537, A15
- Schlegel, D. J., Finkbeiner, D. P., & Davis, M. 1998, *ApJ*, 500, 525
- Schulze, S., Klose, S., Björnsson, G., et al. 2011, *A&A*, 526, A23
- Shao, L., & Dai, Z. G., 2005, *ApJ*, 633, 1027
- Smith, R. J., Melandri, A., Steele, I. A., et al. 2008 *GCN*, 8333
- Soderberg, A. M., Chakraborti, S, Pignata, G., et al. 2010, *Nature*, 463, 513
- Sparre, M., Sollerman, J., Fynbo, J. P. U., et al. 2011, *ApJ*, 735, L24
- Stanek, K. Z., Matheson, T., Garnavich, P. M., et al. 2003, *ApJ*, 591, L17
- Starling, R. L. C., Wiersema, K., Levan, A. J., et al. 2011, *MNRAS*, 411, 2792
- Steele, I. A., Mundell, C. G., Smith, R. J., Kobayashi, S., & Guidorzi, C. 2009, *Nature*, 462, 767
- Tanvir, N. R., Rol, E., Levan, A. J., et al. 2010, *ApJ*, 725, 625
- Taubenberger, S., Pastorello, A., Mazzali, P. A., et al. 2006, *MNRAS*, 371, 1459

- Troja, E., Sakamoto, T., Guidorzi, C., et al. 2012, ApJ, 761, 50
Urata, Y., Zhang, Z. W., Wen, C. Y. et al. 2009, GCN, 9240
Usov, V. V. 1994, MNRAS, 267, 1035
West, J. P., Schubel, M., Haislip, J. et al. 2008 GCN, 8352
Wren, J., Vestrand, W. T., Wozniak, P. R., Davis, H., & Norman, B. 2008 GCN, 8337
Xue, R. R., Fan, Y. Z. & Wei, D. M. 2009, A&A, 498, 671
Yonetoku, D., Murakami, T., Gunji, S. et al. 2011, ApJ, 743, L30
Yuan, F. 2009, GCN, 9224
Zhang, B., Fan, Y. Z., Dyks, J., et al. 2006, ApJ, 642, 354
Zhang, B., Kobayashi, S., & Mészáros, P. 2003, ApJ, 595, 950
Zhang, B. & Mészáros P., 2004, IJMPA, 19, 2385
Zhang, B., Zhang, B. B., Liang, E. W. et al. 2007, ApJ, 655, L25
Zhang, B. B., Zhang, B., Liang, E. W. et al. 2011, ApJ, 730, 141

APPENDIX: TABLE FOR OBSERVATIONS³¹

³¹ THE FOLLOWING MATERIAL ONLY APPEARS ONLINE

TABLE 3
OPTICAL OBSERVATIONS OF GRB 081007.

Instrument	Filter	Mid-time (min)	Exp-time (min)	Mag (AB)	Error	Instrument	Filter	Mid-time (min)	Exp-time (min)	Mag (AB)	Error						
REM	r'	2.94	2.50	16.35	0.06	UVOT	v	7.94	0.42	17.55	0.26						
		5.67	0.01	17.14	0.24			8.36	0.42	17.82	0.32						
		6.32	0.01	17.41	0.31			9.19	0.42	17.67	0.29						
		6.98	0.01	17.11	0.24			9.61	0.42	18.11	0.38						
		7.64	0.01	17.20	0.26			17.32	1.67	18.63	0.29						
		8.29	0.01	17.39	0.31			18.98	1.67	18.96	0.37						
		8.94	0.01	17.28	0.32			20.65	1.67	18.45	0.25						
		H	1.57	0.08	15.41			0.29	White	2.02	0.42	17.08	0.06				
			1.82	0.08	15.00			0.14		2.43	0.42	17.00	0.06				
			2.08	0.08	14.47			0.20		2.85	0.42	17.17	0.07				
			2.38	0.08	14.80			0.12		3.27	0.41	17.37	0.07				
			2.64	0.08	15.09			0.12		12.01	0.16	18.81	0.28				
			2.88	0.08	15.34			0.18		322.75	4.92	20.17	0.15				
			3.40	0.08	15.43			0.19		327.62	4.57	20.27	0.17				
			4.21	0.50	16.11			0.14		1000.44	6.95	21.14	0.28				
	5.53		0.52	16.20	0.14		1753.79	12.97		21.44	0.27						
	10.68		0.50	16.68	0.24		PROMPT	B		1.86	0.33	16.77	0.16				
	16.51		0.85	17.37	0.23					2.34	0.33	16.48	0.17				
	25.67		1.17	17.42	0.21					2.80	0.33	16.94	0.21				
	50.85		1.18	17.90	0.31					6.68	3.42	18.10	0.13				
	RAPTOR		K_s	7.68	0.39					16.80	0.18	19.88	8.28	18.46	0.11		
				12.13	0.59					17.21	0.19	47.06	17.34	19.24	0.15		
				18.85	1.01					17.57	0.17	118.19	52.34	20.13	0.27		
				r'	1.51					0.08	17.06	0.04	V	2.41	0.17	16.51	0.23
					1.66					0.08	16.64	0.03		3.27	0.17	16.71	0.23
		1.90			0.17		16.07	0.02	4.50	0.67	17.15	0.11					
		2.11			0.17		15.93	0.02	6.18	0.67	17.66	0.18					
		2.33			0.17		15.84	0.02	8.57	1.33	17.85	0.12					
		2.55			0.17		15.90	0.02	11.61	1.33	17.89	0.12					
		2.76	0.17		15.92		0.02	14.64	1.33	17.97	0.14						
		2.98	0.17		16.14		0.03	16.13	1.33	17.91	0.14						
		3.20	0.17		16.10		0.03	20.65	1.33	18.06	0.14						
		3.42	0.17	16.47	0.04		22.15	1.33	18.26	0.15							
3.63		0.17	16.51	0.04	26.70	1.33	18.41	0.20									
3.84		0.17	16.50	0.04	35.73	1.33	18.21	0.14									
4.05		0.17	16.65	0.04	37.21	1.33	18.54	0.18									
4.26		0.17	16.93	0.05	38.68	1.33	18.65	0.21									
4.48		0.17	16.75	0.05	49.20	1.33	18.69	0.23									
4.69	0.17	16.79	0.05	64.40	1.33	18.94	0.13										
4.90	0.17	16.73	0.04	r'	2.33	0.75	16.03	0.07									
5.12	0.17	16.99	0.06		6.27	2.67	16.80	0.05									
5.33	0.17	16.97	0.06		39.13	28.00	18.52	0.13									
5.54	0.17	17.34	0.08		902.94	176.00	20.65	0.15									
6.16	0.97	17.14	0.03		i'	1.27	0.33	17.43	0.10								
7.64	1.76	17.43	0.07			2.35	0.67	15.42	0.05								
9.53	1.77	17.93	0.11			3.09	0.50	15.71	0.05								
11.42	1.76	17.90	0.11			4.03	0.67	16.22	0.20								
13.94	3.01	18.30	0.12			5.37	1.33	16.57	0.05								
17.08	3.00	18.61	0.16	7.48		3.33	16.97	0.03									
21.80	6.18	18.75	0.13	12.27		4.00	17.54	0.03									
UVOT	u	11.37	0.33	18.40		0.35	16.78	4.00	17.68	0.03							
		13.87	0.33	18.14		0.29	21.32	4.00	17.96	0.05							
		418.62	4.92	20.34	0.39	25.83	4.00	18.25	0.05								
		423.68	4.92	20.15	0.33	30.38	4.00	18.23	0.05								
		993.28	6.95	20.40	0.35	34.87	4.00	18.17	0.05								
		14.21	0.16	18.19	0.32	39.27	4.00	18.27	0.05								
		v	3.78	0.40	16.77	0.16	43.87	4.00	18.46	0.06							
			4.19	0.42	16.87	0.17	48.37	4.00	18.50	0.05							
			4.61	0.42	17.97	0.35	55.97	8.00	18.42	0.07							
	5.03		0.42	17.31	0.22	64.40	8.00	19.10	0.08								
	5.44		0.42	17.35	0.23	76.85	13.33	18.64	0.05								
	5.86		0.42	18.21	0.41	92.02	13.33	18.77	0.05								
	6.28		0.42	17.60	0.27	108.95	16.00	18.99	0.07								
	6.69		0.42	17.54	0.25	126.90	16.00	19.37	0.08								
	7.11		0.42	17.42	0.24	187.87	49.33	19.14	0.09								
	7.53	0.42	17.85	0.31	1206.90	66.67	21.38	0.12									

TABLE 4
OPTICAL OBSERVATIONS OF GRB 081007 (CONTINUED).

Instrument	Filter	Mid-time (min)	Exp-time (min)	Mag (AB)	Error	
FTN	<i>B</i>	18.03	0.17	19.06	0.31	
		22.93	0.50	19.00	0.22	
		27.33	1.00	19.49	0.21	
		33.60	2.00	19.77	0.21	
		42.80	3.00	19.83	0.18	
		53.95	2.00	19.73	0.19	
		64.13	3.00	19.98	0.18	
		75.30	4.00	20.01	0.18	
		109.78	10.00	20.35	0.15	
		236.48	10.00	20.77	0.17	
		1584.32	30.00	22.66	0.34	
		<i>V</i>	20.38	0.17	18.59	0.14
			84.25	10.00	19.67	0.04
			145.95	10.00	19.69	0.08
			224.45	10.00	20.15	0.06
	1642.58		10.00	21.73	0.26	
	1668.58		15.00	22.51	0.49	
	<i>r'</i>		17.49	0.50	18.21	0.05
			24.27	0.50	18.50	0.06
			29.15	1.00	18.54	0.04
			36.42	2.00	18.75	0.05
		46.57	3.00	18.87	0.03	
		56.75	2.00	19.10	0.04	
		66.90	3.00	19.13	0.06	
		133.94	10.00	19.71	0.05	
		203.04	10.00	19.95	0.05	
		260.67	10.00	19.90	0.05	
		1581.47	30.00	21.60	0.16	
		2981.45	60.00	22.74	0.37	
	<i>i'</i>	21.55	0.17	17.90	0.08	
		25.67	0.50	18.06	0.05	
		31.13	1.00	18.25	0.04	
		39.38	2.00	18.40	0.04	
		51.58	3.00	18.62	0.03	
		59.72	2.00	18.71	0.04	
		71.88	3.00	18.87	0.04	
		121.88	10.00	19.26	0.07	
		190.98	10.00	19.61	0.05	
		248.62	10.00	19.54	0.05	
		1604.16	35.00	21.62	0.15	
		3015.03	60.00	22.56	0.45	
	FTS	<i>r'</i>	1710.34	60.00	21.29	0.18
			3395.84	90.00	22.09	0.38
	VLT	<i>i'</i>	1712.61	30.00	21.41	0.19
			<i>R_c</i>	24163.20	13.70	23.65
			38563.20	2.00	23.79	0.13
			60264.00	6.00	24.14	0.10
		73152.00	6.00	24.39	0.11	
		87566.40	6.00	24.37	0.18	
		97660.80	12.00	24.44	0.12	
		125712.00	27.00	>24.67		
		<i>I_c</i>	60278.40	6.00	23.18	0.10
			73166.40	6.00	23.67	0.11
			87566.40	6.00	24.12	0.22
		97660.80	12.00	23.93	0.16	
		126475.20	21.00	24.29	0.20	
Gemini	<i>g'</i>	24156.00	5.00	24.91	0.19	
	<i>r'</i>	24173.00	5.00	23.89	0.08	
	<i>i'</i>	24179.00	5.00	23.58	0.07	
	<i>z'</i>	24186.00	5.00	23.13	0.09	

NOTE. — Galactic extinction has not been removed.

TABLE 5
OPTICAL OBSERVATIONS OF GRB 090424.

Instrument	Filter	Mid-time (min)	Exp-time (min)	Mag (AB)	Error	Instrument	Filter	Mid-time (min)	Exp-time (min)	Mag (AB)	Error
UVOT	UVW2	13.22	0.32	17.54	0.28	UVOT	v	1.33	0.16	13.82	0.07
		19.94	0.32	17.66	0.29			10.74	0.33	16.88	0.19
UVOT	UVM2	133.50	2.02	19.77	0.38	UVOT	v	13.64	0.33	17.19	0.24
		11.17	0.32	17.39	0.34			17.48	0.33	17.65	0.31
UVOT	UVW1	320.28	13.80	20.04	0.22	UVOT	v	20.35	0.33	17.97	0.39
		603.99	14.76	20.59	0.31			23.21	0.33	17.89	0.37
UVOT	UVW1	11.58	0.33	16.77	0.19	UVOT	v	26.11	0.33	17.79	0.35
		18.30	0.32	17.93	0.34			29.00	0.33	18.75	0.72
UVOT	UVW1	21.17	0.32	17.49	0.28	UVOT	v	31.89	0.32	17.63	0.32
		24.04	0.32	17.69	0.31			34.76	0.32	18.35	0.53
UVOT	UVW1	26.94	0.33	18.49	0.48	UVOT	v	37.66	0.32	17.58	0.30
		29.82	0.32	18.20	0.41			200.71	4.92	19.55	0.35
UVOT	UVW1	32.71	0.33	18.66	0.52	UVOT	v	203.53	0.52	19.77	1.33
		35.58	0.33	17.56	0.28			1.62	0.17	15.03	0.05
UVOT	UVW1	94.17	3.28	18.79	0.19	UVOT	White	1.78	0.17	15.39	0.05
		417.97	11.20	20.52	0.33			1.95	0.17	15.27	0.05
UVOT	u	5.15	0.17	16.00	0.13	UVOT	White	2.12	0.17	15.46	0.05
		5.32	0.17	16.29	0.15			2.28	0.17	15.57	0.06
UVOT	u	5.48	0.17	16.25	0.15	UVOT	White	2.45	0.17	15.43	0.05
		5.65	0.17	16.23	0.14			2.62	0.17	15.55	0.06
UVOT	u	5.82	0.17	16.36	0.15	UVOT	White	2.78	0.17	15.66	0.06
		5.98	0.17	16.35	0.15			2.95	0.17	15.70	0.06
UVOT	u	6.15	0.17	16.73	0.19	UVOT	White	3.12	0.17	15.77	0.06
		6.32	0.17	16.46	0.16			3.28	0.17	15.87	0.06
UVOT	u	6.48	0.17	16.47	0.16	UVOT	White	3.45	0.17	15.99	0.06
		6.65	0.17	16.75	0.19			3.62	0.17	16.11	0.06
UVOT	u	6.82	0.17	16.38	0.15	UVOT	White	3.78	0.17	16.06	0.06
		6.98	0.17	16.87	0.20			3.95	0.16	16.23	0.07
UVOT	u	7.15	0.17	16.76	0.19	UVOT	White	9.78	0.12	17.26	0.12
		7.32	0.17	16.63	0.18			9.95	0.17	17.55	0.13
UVOT	u	7.48	0.17	17.05	0.22	UVOT	White	10.12	0.04	17.77	0.29
		7.65	0.17	16.73	0.18			12.62	0.07	17.51	0.19
UVOT	u	7.82	0.17	16.68	0.18	UVOT	White	12.78	0.17	17.66	0.13
		7.98	0.17	16.55	0.17			12.95	0.10	18.00	0.21
UVOT	u	8.15	0.17	17.00	0.22	UVOT	White	19.45	0.17	18.37	0.21
		8.32	0.17	16.91	0.20			19.62	0.15	18.11	0.18
UVOT	u	8.48	0.17	16.83	0.19	UVOT	White	22.28	0.14	18.28	0.21
		8.65	0.17	16.63	0.17			22.45	0.17	18.07	0.17
UVOT	u	8.82	0.17	17.29	0.25	UVOT	White	25.28	0.33	18.31	0.14
		8.98	0.17	16.78	0.19			28.17	0.32	18.06	0.13
UVOT	u	9.15	0.16	16.84	0.20	UVOT	White	31.06	0.33	18.14	0.13
		11.82	0.09	17.07	0.30			33.93	0.32	18.29	0.15
UVOT	u	11.98	0.17	17.19	0.23	UVOT	White	36.81	0.33	18.16	0.13
		12.15	0.08	17.30	0.37			110.47	2.61	19.26	0.11
UVOT	u	18.70	0.33	17.41	0.19	UVOT	White	453.22	30.00	19.67	0.02
		24.45	0.33	17.53	0.20			573.28	30.00	19.91	0.08
UVOT	u	27.35	0.33	17.73	0.23	UVOT	White	499.33	30.00	19.66	0.04
		33.12	0.32	18.65	0.42			25435.85	30.00	21.86	0.11
UVOT	u	35.99	0.32	18.04	0.28	FTN	r'	480809.88	30.00	21.65	0.11
		96.14	0.44	18.01	0.24			482086.00	30.00	22.03	0.15
UVOT	u	103.97	3.28	19.12	0.19	UVOT	White	483666.35	30.00	21.78	0.15
		500.30	4.92	20.01	0.31			9360.01	6.00	22.00	0.10
UVOT	u	505.37	4.92	20.23	0.37	UVOT	White	26619.71	6.00	22.08	0.15
		510.43	4.92	19.86	0.27			38151.23	6.00	22.13	0.08
UVOT	b	9.51	0.33	17.32	0.14	UVOT	White	71316.72	6.00	21.90	0.35
		12.39	0.33	17.46	0.14			104267.52	3.00	22.50	0.21
UVOT	b	19.12	0.32	17.84	0.18	UVOT	White	9344.68	4.00	21.65	0.08
		21.98	0.32	18.06	0.21			9349.57	4.00	21.56	0.08
UVOT	b	24.89	0.33	18.30	0.24	UVOT	White	9354.13	4.00	21.66	0.08
		27.77	0.33	18.56	0.29			26627.66	4.00	21.80	0.10
UVOT	b	30.64	0.33	18.36	0.26	UVOT	White	26634.29	4.00	21.79	0.09
		33.53	0.32	18.75	0.34			38156.93	4.00	21.78	0.06
UVOT	b	36.40	0.32	18.07	0.21	UVOT	White	38161.57	4.00	21.77	0.07
		107.40	3.28	19.79	0.24			71322.34	4.00	21.88	0.14
UVOT	b	229.69	2.41	20.13	0.37	UVOT	White	71326.81	4.00	21.85	0.16
		515.53	4.92	20.29	0.30			104238.34	4.00	21.86	0.13
UVOT	b	519.06	1.92	20.80	0.74	UVOT	White	104247.08	4.00	21.85	0.13
		CAHA	J	1589029.99	212.00			21.60	0.11		
CAHA	H	1589080.06	47.00	21.21	0.32						

NOTE. — Galactic extinction has not been removed.